EUROPEAN ORGANIZATION FOR NUCLEAR RESEARCH

CERN/EP 83-192
14 December 1983

TOPOLOGICAL CROSS SECTIONS AND CHARGED PARTICLE MULTIPLICITIES IN pp INTERACTIONS AT 360 GeV/c

EHS - RCBC Collaboration

Bombay[1], CERN[2], Genova[3], Innsbruck[4], Japan-UG[5], Madrid[6], Mons[7], Rutgers[8], Serpukhov[9], Tennessee[10], Vienna[11] Collaboration

J.L. Bailly[7], S. Banerjee[1], W. Bartl[11], F. Bruyant[2], W.M. Bugg[10], C. Caso[2], Y. Chiba[5(d)], R. Contri[3], F. Crijns[(*)], R. Di Marco[8], B. Epp[4], A. Ferrando[6], F. Fontanelli[3], A. Gurtu[1], R. Hamatsu[5(a)], E.L. Hart[10], P. Herquet[7], J. Hrubec[2], N. Khalatjan[9(+)], E. Kistenev[9], I. Kita[5(b)], D. Kuhn[4], A. Kursonenko[9], J. MacNaughton[11], J.C. Marin[2], M. Markytan[11], I.S. Mittra[(**)], L. Montanet[2], G. Neuhofer[11], N. Ohshima[5(a)], Y. Petrovikh[9], R. Plano[8], P. Porth[11], R. Raghavan[1], T. Rodrigo[6], A.H. Rogers[10], J. Salicio[6], K. Shankar[1], J.B. Singh[(**)], S. Squarcia[3], P. Stamer[8], D. Toet[(***)], U. Trevisan[3], P. van Hal[(*)], C. Willmott[6] and G. Zholobov[9]

1 Tata Institute of Fundamental Research, Bombay, India
2 CERN, European Organization for Nuclear Research, Geneva, Switzerland
3 University of Genova and INFN, Italy
4 Inst. für Experimentalphysik, Innsbruck, Austria(++)
5(a) Tokyo Metropolitan University, Tokyo, Japan
(b) Tokyo University of Agriculture and Technology, Tokyo, Japan
(c) Chuo University, Tokyo, Japan
(d) Hiroshima University, Hiroshima, Japan
6 Junta de Energia Nuclear, Madrid, Spain
7 Université de l'Etat, Faculté des Sciences, Mons, Belgium
8 Rutgers University, New Brunswick, USA
9 I.H.E.P., Serpuhkov, USSR
10 University of Tennessee, Knoxville, USA
11 Inst. für Hochenergiephysik, Vienna, Austria(++)
(*) University of Nijmegen and NIKHEF Nijmegen, the Netherlands
(**) Punjab University, Chandigarh, India
(***) NIKHEF, Amsterdam, the Netherlands
(+) Also at Erevan Phys. Institute, Armenian Acad. Science, USSR

Submitted to Zeitschrift für Physik C

(++) Supported by Fonds zur Förderung der Wissensch. Forschung.

ABSTRACT

Using data obtained with EHS equipped with the Rapid Cycling Bubble Chamber (RCBC) exposed to a proton beam of 360 GeV/c, we calculate topological cross sections. We present in great detail the procedure and the techniques used to correct raw data. Finally, we give multiplicity moments and multiplicity correlations and we compare the values obtained in our experiment, together with data at other energies, with different models.

1. INTRODUCTION

In the CERN program of investigation of high energy hadronic phenomenology using the European Hybrid Spectrometer (EHS) [1], the experiment NA23, which the data discussed in this paper derive from, was conceived to analyze diffractive interactions at the highest SPS energy. Protons were chosen as incident particles to exploit the symmetry of the initial state, reducing the necessary time of exposure.

A first analysis of strange particle diffractive production compared with charm production will be published elsewhere [2].

The special features of the EHS, which includes two gamma detectors, allow π^{o} detection over a wide spectrum of Feynman-x and open the possibility of studying π^{o} inclusive reactions [3].

This paper is aimed to present the topological cross sections as well as the usual multiplicity parameters. A description of the bubble chamber flash trigger is also included.

2. THE EXPERIMENTAL APPARATUS

The experimental set-up for NA23 is shown schematically in fig. 1. The RCBC, filled with hydrogen, was exposed to a proton beam of 360 GeV/c coming from the H2 beam line. The beam was defined by two multiwire proportional chambers U1 and U3, each equipped with five wire planes for the precision measurement of beam coordinates.

RCBC has a diameter of 80 cm and a depth of 40 cm and was placed in a magnet field of 3.0 T, supplied by the superconducting magnet M1 with an operating current of 4000 A. The exit window of 2 mm stainless steel and the vacuum tank window of 3 mm Al/glass fibre correspond to 0.146 L_{rad} and 0.0255 L_{coll}. The expansion system is characterized by the following values:

Static pressure:	5.0 bar;
Vapour pressure at 25°K:	3.2 bar;
Expanded pressure:	1.1 bar;
Flash delay:	1.0 ÷ 1.5 ms;
Width of expansion pulse	11 ms.

The time gate for RCBC being ready to accept beams was 0.5 ms. The chamber working frequency, not constant during the experiment, was in most circumstances 10 Hz.

The downstream spectrometer consists of a six-plane multi-proportional wire chamber W2 (0.9 X 1.6 m^2) with 2 mm sense wire spacing and six drift chamber D1, D2, D3 (4 X 2 m^2), D4, D5, D6 (2 X 1.3 m^2). Each drift chamber is composed of four modules of one sense wire plane (wire spacing = 4.8 cm) and two planes of field shaping wires each with wire angles of ± 13° and ± 7° from horizontal. The chambers were filled with a mixture of argon and ethane with a small admixture of ethanol. Typical voltages at the sense and field wires were -1.6 and 2.7 kV respectively. The maximum drift time was ~ 500 ns.

At a distance of 16.6 ÷ 18.6 m from the centre of RCBC, the C-shaped magnet M2 provided a field of 1.5 T by means of a current of 1000 A. Its aperture was 0.4 X 1.0 m^2.

The following particle identification devices were installed:

(a) An 18-cell Silica Aerogel Detector for the identification of π, K, and p in the momentum range 2÷4 GeV/c;

(b) A 4 X 2 X 5 m^3 pictorial drift chamber ISIS, filled with Ar/CO_2, with maximally 120 kV at the top and bottom with respect to a central horizontal wire plane, with 1.6 cm distance between consecutive channels, for ionization sampling and determining the relativistic ionization rise.

Our set-up was finally completed by an intermediate gamma detector at 14 m consisting of 1122 cells with 14 ÷ 15 radiation lengths and a forward gamma detector at 39 m consisting of 140 glass blocks organized in a converter plane (4.5 radiation lengths) and an absorber plane (24 radiation lengths) with 375 hodoscope fingers in between.

3. THE INTERACTION TRIGGER

In order to discriminate between non-interacting beams and elastic and target diffraction dissociation events with fast forward going particles produced with small momentum transfers, two trigger hodoscopes were positioned at 12.5 m downstream the centre of RCBC. The configuration of the trigger system is illustrated in fig. 2. The horizontal trigger hodoscope (ITH) consisting of 26 horizontal scintillator strips, 20 of 2 cm width and 6 of 15 cm width, was used to trigger on the multiplicity of secondary particles equal to or larger than one. The additional vertical trigger hodoscope (ITV) consisted of a middle finger of 0.6 cm width, flanked by two strips of 5 cm width each. The dimensions and the layout of the trigger hodoscopes have been optimized by Monte-Carlo studies using diffractive reactions.

The beam was focused onto the middle finger ITV (2) of the vertical trigger hodoscope, with a FWHM ~ 3.5 mm.

The trigger conditions can be summarized as

$$\text{BEAM} * \{[\text{ITH } (n \geq 2)] \text{ or } [\text{ITV } (n \geq 1) \text{ and } \overline{\text{ITV } (2)}]\} \ .$$

The first part accepts reactions with at least two charged particles hitting ITH; the second part was intended to pick up reactions with one fast forward going particle, required not to be a beam particle.

The beam trigger was defined by

$$\text{BEAM} = \text{T1} * \text{T2} * \overline{(\text{V1} + \text{V2})}$$

where T_1, T_2, V_1 and V_2 are hodoscopes placed on the beam line upstream the bubble chamber (fig. 2). The useful beam spread was consequently ~ 5 mm in the horizontal plane at the centre of RCBC.

Because of window and downstream interactions the number of empty pictures comes out to be as high as 50%.

4. THE DATA SAMPLE

The event sample used in this paper is based on about 17 K pictures from a first exposure of 160 K pictures. A second exposure, in the same experimental conditions, gave subsequently some further 180 K pictures.

The fiducial length in the bubble chamber was ~ 75 cm and the minimum acceptable length of beam tracks ~ 0.02 cm on the film.

Two upstream wire chambers were used to predict the transverse position of the interaction giving the trigger; then the scanning efficiency was ~ 100% for the detection of primaries, but varied between 70% and 100% for V°/γ vertices as a function of the primary multiplicity and of the distance from the production point. The uncorrected number of events of the different charged multiplicities are shown in table 1. To these rough numbers the usual corrections were applied.

4.1 Odd topologies

They were shared between neighbouring topologies proportionally to the corresponding populations.

4.2 Unseen V°/γ

The distribution of the seen decays as a function of the decay length is shown in fig. 3 in which the numbers are corrected for scanning efficiencies. The exponential extrapolation to zero decay length indicates a total loss of 137 decays, whose distribution among the different topologies is given in table 2.

4.3 Dalitz pairs

The observed electrons (if not an obvious δ-ray) and the non-observed Dalitz pairs were included in the prong counts. To correct for, the empirical rule [4]

$$\langle n_{\pi^o} \rangle = \langle n_{\pi^-} \rangle + 0.4$$

for the estimated average π^o-multiplicity was applied, taking then into account a probability of a Dalitz pair creation of 1.213% [5].

4.4 Trigger Inefficiency

The losses associated with possible trigger inefficiencies for low multiplicity events are difficult to estimate. The counters themselves were assumed to have a 100% efficiency, so most of the losses come from the event configuration.

The reactions

$$pp \to pp, \tag{1}$$

$$pp \to p(p\,\pi^o), \tag{2}$$

$$pp \to (p\,\pi^o)p, \tag{3}$$

were simulated by a Monte-Carlo program. The choice of reaction (1) is obvious: a slope of 10.6 $(GeV/c)^{-2}$ for the t-distribution [6] was used. The reactions (2) and (3) present the main characteristical features of the two-prong inelastic events. For the generation of the diffractive-type events the semi-empirical dependence of the t-slope on the effective mass of the recoil system suggested in ref. [7] was chosen. The position of the vertices in the bubble chamber was generated according to the real distribution observed at the scanning. The Monte-Carlo t-distributions are shown in fig. 4, where the dashed regions correspond to events satisfying the trigger conditions. We obtain for the three reactions the following percentages of losses due to the geometrical limitations of our trigger system

$$\varepsilon_1 = 28.0\%;\ \varepsilon_2 = 21.7\%;\ \varepsilon_3 = 7.5\% \ . \tag{4}$$

Very similar inefficiencies were found generating diffractive events with $p \to (n\pi^+)$ both from beam and target fragmentation.

The value $\varepsilon_{el} = 28.0\%$ was eventually assumed for the loss of elastic two-prong events, while for inelastic we took

$$\varepsilon_{in} = 14.5\% \ . \tag{5}$$

In the same way we found a trigger inefficiency not higher than a few percent for four-prong events; this inefficiency was therefore neglected in the cross section calculation.

4.5 Scanning losses

Additional losses of two-prong events are connected to unseen short recoils. Imposing different cuts on a minimum detectable length of the recoiling proton, the Monte-Carlo events of the previous section were used to compute the probability for an event to satisfy the trigger conditions while being lost at the scanning level. It was found

$$\alpha_{el} = 0.046 \; ; \; \alpha_{in} = 0.086. \qquad (6)$$

4.6 Misidentified secondaries

A correction was also applied for misidentification of secondary interactions sitting on fast tracks from an undetectable two prong event. This occurrence was determined from Monte-Carlo generation to concern 6.0% of the two-prongs with unseen recoiling proton.

5. TOPOLOGICAL CROSS SECTIONS

The corrected topology break-up (calculated using the procedure described in the Appendix) as well as the corresponding topological cross sections are summarized in table 1.

Owing to the difficulty to compute the total length of the beam track in an experiment which was not designed for this purpose, we normalized our cross sections using the values for $\sigma_{tot} = (39.80 \pm 0.50)$mb and $\sigma_{el} = (7.00 \pm 0.31)$ mb as derived interpolating among the available published data.

Fig. 5 shows the usual energy dependence of the pp topological cross sections including the data listed in table 2. Our data extrapolate smoothly the tendencies observed at lower energies. Some small

discrepancies between our data and those at 405 GeV [8] are probably explained by the limited statistics of that. We observe that at our energy the cross sections for the final states with up to ten charged particles have already reached their maxima while for higher topologies the cross sections are still increasing.

The multiplicity distribution is compared in fig. 6 with the predictions from the KNO-scaling hypothesis. Besides our data, in the figure also appear results from pp experiments at 100, 147, 205, 303, 405 GeV/c incident momenta [9]. The empirical superimposed curve is the one proposed by Slattery [10]:

$$c(z) = (3.79\ z + 33.7\ z^3 - 6.64\ z^5 + 0.332\ z^7)\ \exp(-3.04\ z) \quad (7)$$

with the scaling parameter $z = n/\langle n \rangle$ (table 3).

6. MULTIPLICITY MOMENTS AND MULTIPLICITY CORRELATIONS

The various charge multiplicity parameters both for all tracks and for negative tracks only have been calculated giving results of table 3. Once more our points lie well in between the data measured at different energies. This is shown in fig. 7 for the dependence of the average multiplicity $\langle n \rangle$ on $\sqrt{s}$. The curve is the parametrization suggested in [11]

$$\langle n(s) \rangle = -8.044 + 8.149\ s^{0.11}\ , \quad (8)$$

giving at our energy the prediction $\langle n \rangle = 8.65$ to be compared to the experimental value $\langle n \rangle = 9.06 \pm 0.09$ of table 3.

Following the ideas of the constituent quark model which proposes the functional dependence

$$C(x) = x^a\ (1 - x)^b / B(a + 1, b + 1) \quad (9)$$

for the x-distribution of the colliding constituent in the overall c.m. system, it was derived [11] that the observed charge multiplicity can

be expressed in a form directly related to the parameters of the structure function C(x):

$$\langle n(s)\rangle = -6.07 + 9.259\, g(a,b)\, s^{0.11}\ , \qquad (10)$$

where

$$g(a,b) = [\Gamma(a+b+2)\ \Gamma(a+1.11)/(\Gamma(a+1)\ \Gamma(a+b+2.11)]^2 . \qquad (11)$$

The value of the function g(a,b) , as calculated from our data, turns out to be 0.79. It is interesting to compare this result to the value of 0.5 obtained using for a,b the popular values.

$$a = -1/2 \qquad b = 3 \qquad \text{for u,d quarks.}$$

In fig. 8 we compare the behaviour of $\langle n\rangle$ from πp and pp interactions for $p_{Lab} \geq 100$ GeV/c. The differences between pairs of points at the same energy have been investigated in terms of several models [11,12], assuming energy dependent mechanisms. In general they are able to predict for the difference $\langle n_\pi\rangle - \langle n_p\rangle$ a value of $0.3 \div 0.4$ at high energies. On the contrary, using our data such a difference turns out to be -0.23.

The well-known linear dependence [13] of the dispersion D on $\langle n\rangle$ is shown in fig. 9. The solid line is described by the equation [14]

$$D(\langle n\rangle) = 0.575\ (\langle n\rangle - 0.946). \qquad (12)$$

In fig. 10 the first normalized moments C_k of the charge multiplicity distribution are displayed as a function of the incident momentum. The distributions are well fitted by linear functions indicating that the C_k's behave approximately as ℓn s; the exact KNO scaling would require constant with s values.

Among the remaining possible multiplicity parameters we show in fig. 11 the Mueller correlation coefficients f_2 and f_3 for interactions in the energy range 100-400 GeV. The first one shows that at our energy the charge multiplicity distribution is definitely broader than a Poisson-like as suggested by eq. 12.

7. CONCLUSIONS

The energy dependence of the topological cross sections is such that at our energy a maximum is well developed for all multiplicities lower than 12, while for higher multiplicities the cross sections are still increasing. The results obtained show that the unavoidable low multiplicity loss of our trigger is kept at a sufficiently good level and can be fully recovered.

The multiplicity distribution is well described by the Slattery's parameterisation, showing a rather good KNO scaled behaviour. The KNO requirements are not completely fulfilled as it can be observed from the slight dependence on energy of the first normalized moments of the multiplicity distribution.

Average multiplicity as a function of energy is found to be described by a simple power law derived from a constituent quark model. The linear dependence of the dispersion D on $\langle n \rangle$ is confirmed.

APPENDIX

We describe here the technique we used to determine the topological cross sections given in table 1.

Having worked on the uncorrected number of events taking into account odd topologies, unseen V^o/γ and Dalitz pairs using the criteria discussed in the text, we tried to use the information from Monte-Carlo events concerning the trigger efficiency and the unseen two-prongs.

In what follows we shall use the symbols:

$\beta = 0.06$	probability of an unseen two-prong event to have a secondary interaction;
$\alpha_{el} = 0.046$	probability of an elastic two-prong event not to be seen due to a short recoiling proton;
$\alpha_{in} = 0.086$	probability of a not visible inelastic two-prong event;
$\varepsilon_{el} = 0.28$	probability of trigger failure for elastic events;
$\varepsilon_{in} = 0.145$	probability of trigger failure for two-prong inelastic events;
N_{2k}^{seen}	number of seen 2k-prong events;
N_{2k}	number of true 2k-prong events;
N_2^{el}; N_2^{in}	number of elastic and inelastic 2-prong events;
σ_{2k}; σ_{tot}	topological and total cross sections.

We considered first the case of 2k-prongs (k > 1). We have:

$$N_{2k}^{seen} = N_{2k}\left[1 + \frac{\sigma_2}{\sigma_{tot}} \beta\, \alpha_{el}(1-\varepsilon_{el})\right] + \frac{\sigma_{2k}}{\sigma_{tot}} \beta\, [\alpha_{in}(1-\varepsilon_{in})-\alpha_{el}(1-\varepsilon_{el})]N_2^{in}, \quad (A1)$$

where the secondary interactions of unseen two-prongs have been shared among different topologies proportionally to the cross sections. It is easy to realize that the corrective terms are much smaller than the first one and therefore we assumed $N_{2k} = N_{2k}^{seen}$.

To determine the correct number of two-prong events we need to normalize our data to two known cross sections. Among the several possibilities we choosed to use

$$\sigma_{tot} = (39.80 \pm 0.50)\text{mb} \quad \text{and} \quad \sigma_{el} = (7.00 \pm 0.31)\text{mb}.$$

Indicating with p_{el} (p_{in}) the probability for an elastic (inelastic) two-prong to be seen

$$p_{el(in)} = 1 - [\alpha_{el(in)} + \varepsilon_{el(in)} - \alpha_{el(in)}\, \varepsilon_{el(in)}] \tag{A2}$$

we remain with a linear system of two equations

$$\begin{cases} N_2^{el}\, p_{el} + N_2^{in}\, p_{in} = N_2^{seen}, \\ \dfrac{N_2^{el}}{\sigma_{el}} = \dfrac{(N_4 + N_6 + N_8 + \ldots.) + N_2^{el} + N_2^{in}}{\sigma_{tot}}, \end{cases} \tag{A3}$$

from which the data of table 1 are derived.

REFERENCES

[1] M. Aguilar-Benitez et al., Nucl. Instr. and Meth. 205 (1983) 79.

[2] Bombay-CERN-Genova-Innsbruck-Japan UG-Madrid-Mons-Rutgers-Serpukhov-Tennessee-Vienna, EHS-RCBC Collaboration, Strange particle production in 360 GeV/c pp interactions using the European Hybrid Spectrometer, submitted to the International Conference on High Energy Physics, Brighton (1983).

[3] Bombay-CERN-Genova-Innsbruck-Japan UG-Madrid-Mons-Rutgers-Serpukhov-Tennessee-Vienna, EHS-RCBC Collaboration. Inclusive π^{o} production in 360 GeV pp interactions using the European Hybrid Spectrometer, submitted to Zeitschrift für Physik C.

[4] A. Wroblewski, Review of experimental data on multiparticle hadronic reactions, Kaysersberg, June 1977.

[5] M. Roos et al., Review of particle properties, Phys. Lett. 111B (1982) 1.

[6] A. Firestone et al., Phys. Rev. 10 (1974) 2080.

[7] J. Biel et al., Phys. Rev. Lett. 36 (1976) 504.

[8] C. Bromberg et al., Phys. Rev. Lett. 31 (1973) 1563.

[9] 100 GeV, W.M. Morse et al., Phys. Rev. D7 (1977) 66;
147 GeV, D. Brick et al., Phys. Rev. D25 (1982) 2794;
205 GeV, S. Barish et al., Phys. Rev. D9 (1974) 2689;
303 GeV, A. Firestone et al., Phys. Rev. D10 (1974) 2080;
405 GeV, C. Bromberg et al., Phys. Rev. Lett. 31 (1973) 1563.

[10] P. Slattery, Phys. Rev. Lett. 24 (1972) 1624.

[11] F. Takagi, TU/82/240 (1982) unpublished.

[12] V.V. Anisovich, Sov. Journ. of Nucl. Phys. 26 (1977) 571;
M.A. Cirit, Phys. Lett. 82B (1979) 123;
W.M. Morse et al., Phys. Rev. D15 (1977) 66;
C. Pajares and R. Pascual, Nucl. Phys. B137 (1978) 390.

[13] A. Wroblewski, Acta Physica Polonica B4 (1973) 857.

[14] W. Thomé et al., Nucl. Phys. B129 (1977) 365.

TABLE CAPTIONS

Table 1 Topological cross sections for pp interactions at 360 GeV/c (EHS-NA23).

Table 2 Neutral decay losses for different primary multiplicities. Percentages are defined with respect to the primary vertices.

Table 3 Multiplicity parameters for pp interactions at 360 GeV/c (EHS-NA23).

TABLE 1

Prongs	Uncorrected number of events	Corrected number of events	Cross sections (mb)
2 tot	1320	1899	9.09 ± 0.52
2 el		1462	7.00 ± 0.31
2 in		437	2.09 ± 0.36
3	18		
4	891	919	4.40 ± 0.16
5	13		
6	1059	1110	5.31 ± 0.18
7	42		
8	1178	1243	5.95 ± 0.19
9	12		
10	1035	1043	5.00 ± 0.17
11	12		
12	858	845	4.05 ± 0.15
14	542	554	2.65 ± 0.12
16	346	322	1.54 ± 0.09
18	187	185	0.89 ± 0.07
20	114	108	0.52 ± 0.05
22	58	54	0.26 ± 0.04
24	23	23	0.11 ± 0.02
26	10	6	0.03 ± 0.01
≥ 13 (odd)	40		
TOTAL	7758		39.80 ± 0.50

TABLE 2

Mul	2	4	6	8	10	12	14	16	18	20	TOTAL
Lost V^o/γ's	-	-	6	37	32	16	29	6	7	4	137
Percent	-	-	0.55	3.15	3.14	1.84	5.4	1.8	3.65	3.45	1.77

TABLE 3

Parameter	All charged tracks	Neg charged tracks only
$\langle n \rangle$	9.06 ± 0.09	3.53 ± 0.05
$\langle n^2 \rangle$	102.24 ± 1.62	17.50 ± 0.32
$\langle n(n-1) \rangle$	93.18 ± 1.53	13.97 ± 0.27
D	4.49 ± 0.05	2.25 ± 0.03
$\langle n \rangle / D$	2.02 ± 0.04	1.57 ± 0.03
f_2	11.11 ± 0.52	1.51 ± 0.14
f_3	14.65 ± 2.64	-0.94 ± 0.39
$\gamma_3 = \mu_3/D^3$	0.63 ± 0.03	0.63 ± 0.03
$\gamma_4 = \mu_4/D^4$	3.18 ± 0.07	3.18 ± 0.07
$C_2 = \langle n^2 \rangle / \langle n \rangle^2$	1.25 ± 0.01	1.41 ± 0.02
$C_3 = \langle n^3 \rangle / \langle n \rangle^3$	1.81 ± 0.03	2.38 ± 0.06
$C_4 = \langle n^4 \rangle / \langle n \rangle^4$	2.97 ± 0.08	4.60 ± 0.18

FIGURE CAPTIONS

Fig. 1 Set-up of the European Hybrid Spectrometer (EHS) for the 360 GeV/c pp experiment EHS-NA23. The Rapid Cycling Bubble Chamber (RCBC), the magnets M1 and M2, the Multi Wire Proportional Chamber (MWPC) W2, the drift chambers D1, D2, D3, D4, D5, D6, the Silica Aerogel Detector (SAD), the pictorial drift chamber ISIS and the Intermediate and Forward Gamma Detectors (IGD) and (FGD) are shown.

Fig. 2 Sketch of the interaction trigger configuration. See text for a description of the logic.

Fig. 3 Neutral decay-primary vertex distance for all multiplicities. The solid line is the result of an exponential fit.

Fig. 4 Monte-Carlo generated t-distributions for the reactions (1-3) of the text. Dashed regions correspond to events satisfying the trigger conditions. $d\sigma/d|t|$ is given in arbitrary units.

Fig. 5 Energy dependence of the topological cross sections for proton-proton interactions at high energies. The hand-drawn curves are only intended to guide the eye.

Fig. 6 Multiplicity distribution for pp interactions at several energies. The curve is one of the many fits proposed [10].

Fig. 7 Energy dependence of the mean charge multiplicity. The curve corresponds to eq. (8) of the text.

Fig. 8 Energy dependence of the average charge multiplicity for pp (dots) and πp (crosses) interactions. Current models predict a difference of $0.3 \div 0.4$ and eventually a cross-over at higher energies.

Fig. 9 The dispersion D vs the mean multiplicity. The solid line is the representation of formula (12).

FIGURE CAPTIONS (Cont'd)

Fig. 10 The first normalized moments C_k of the multiplicity distribution as a function of the laboratory momentum. The lines are the results of linear fits.

Fig. 11 The correlation parameters f_2 and f_3 as a function of $\sqrt{s}$ for pp interactions at FNAL and SPS energies.

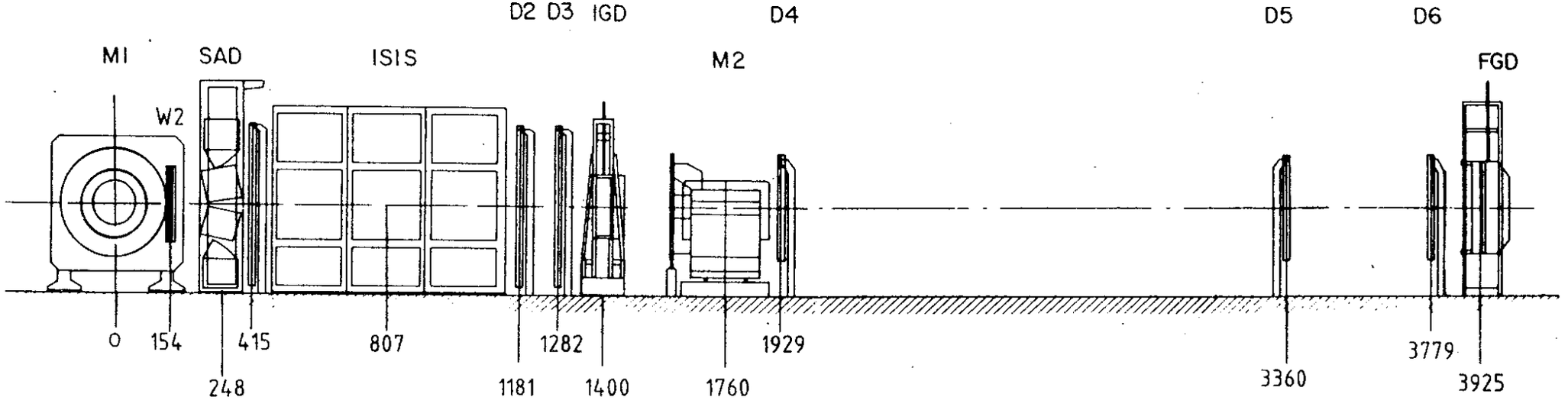
D2 D3 IGD
D4
D5
D6
M1
SAD
ISIS
M2
FGD
W2
0
154
248
415
807
1181
1282
1400
1760
1929
3360
3779
3925

Fig. 1

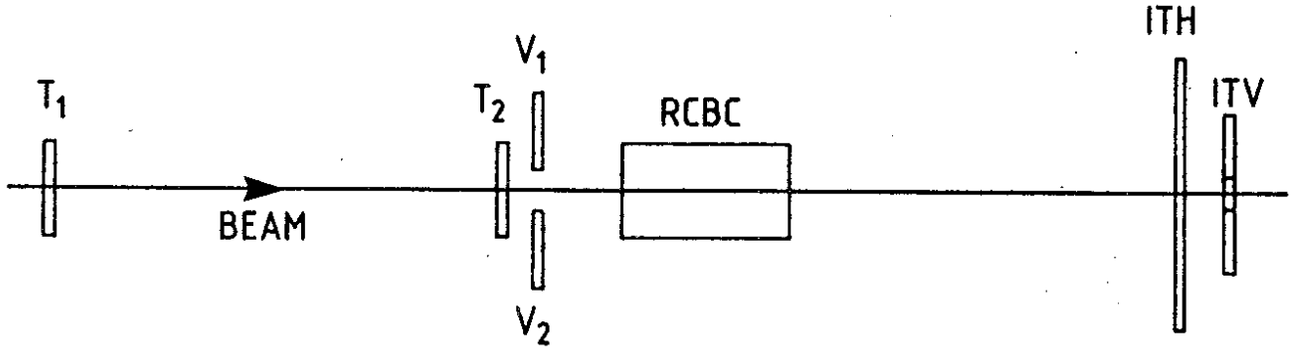

Fig.2

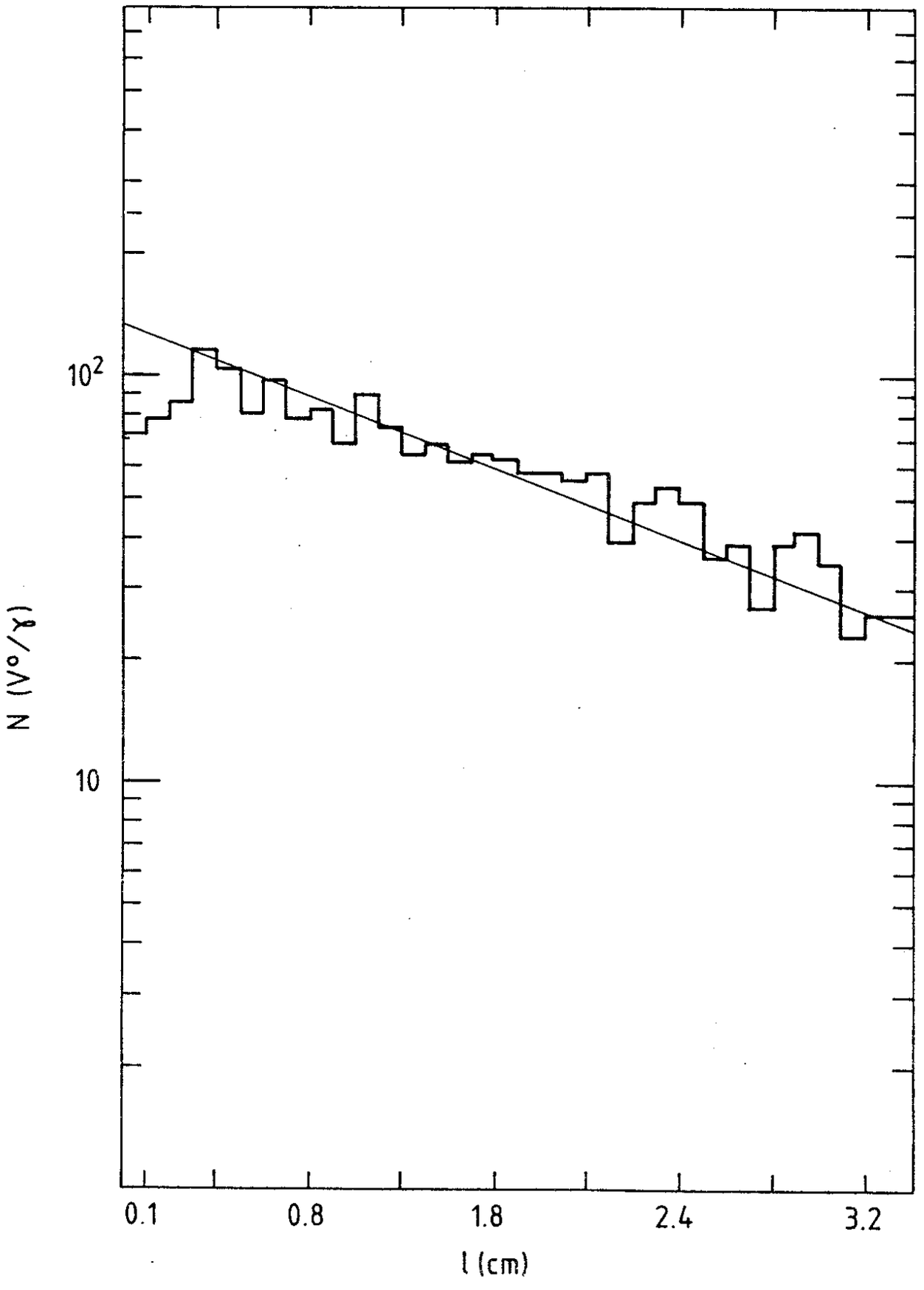

Fig.3

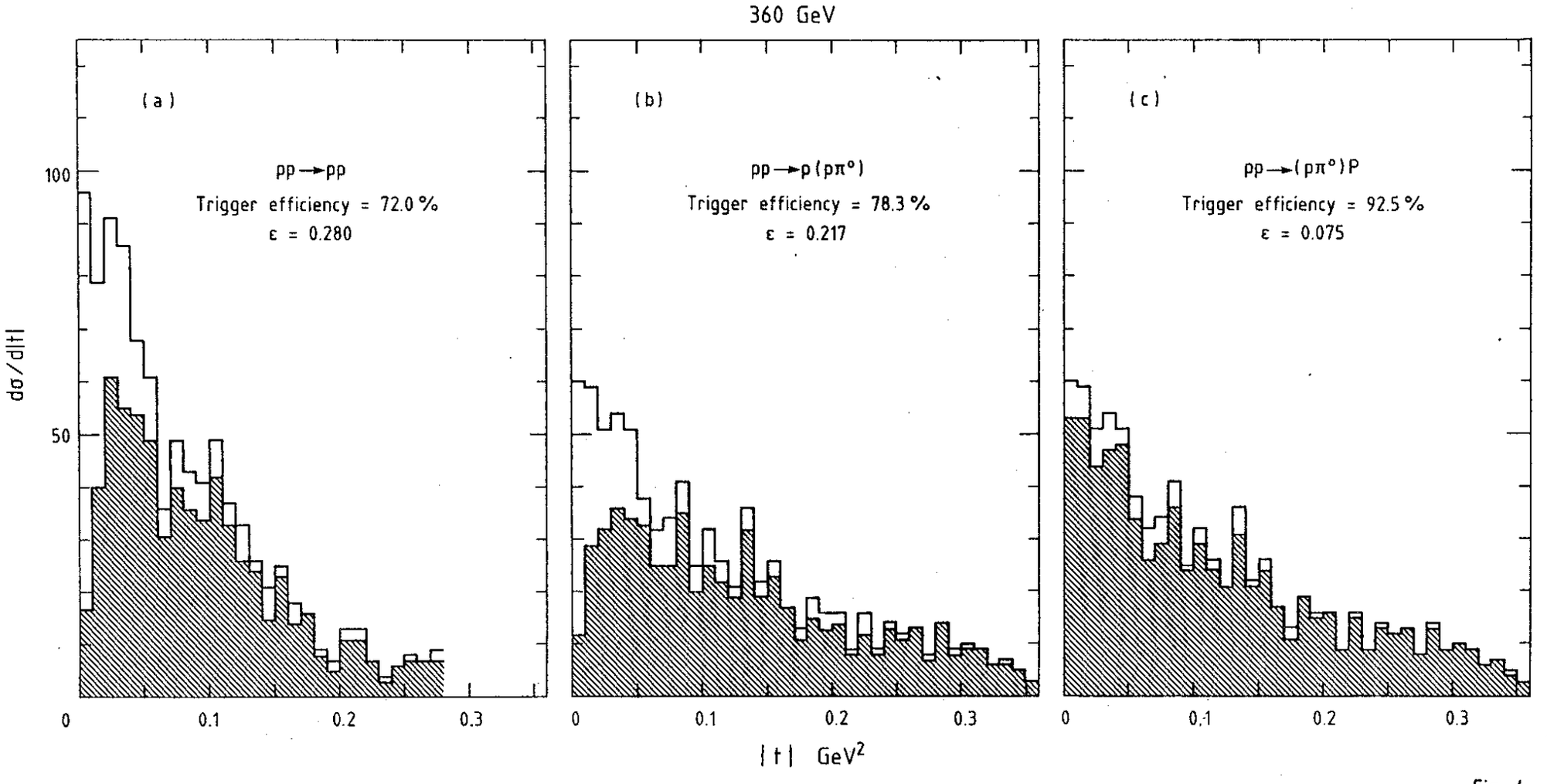
360 GeV
(a)
pp→pp
Trigger efficiency = 72.0 %
ε = 0.280
(b)
pp→p(pπ°)
Trigger efficiency = 78.3 %
ε = 0.217
(c)
pp→(pπ°)P
Trigger efficiency = 92.5 %
ε = 0.075
dσ/d|t|
100
50
0
0.1
0.2
0.3
|t| GeV²

Fig. 4

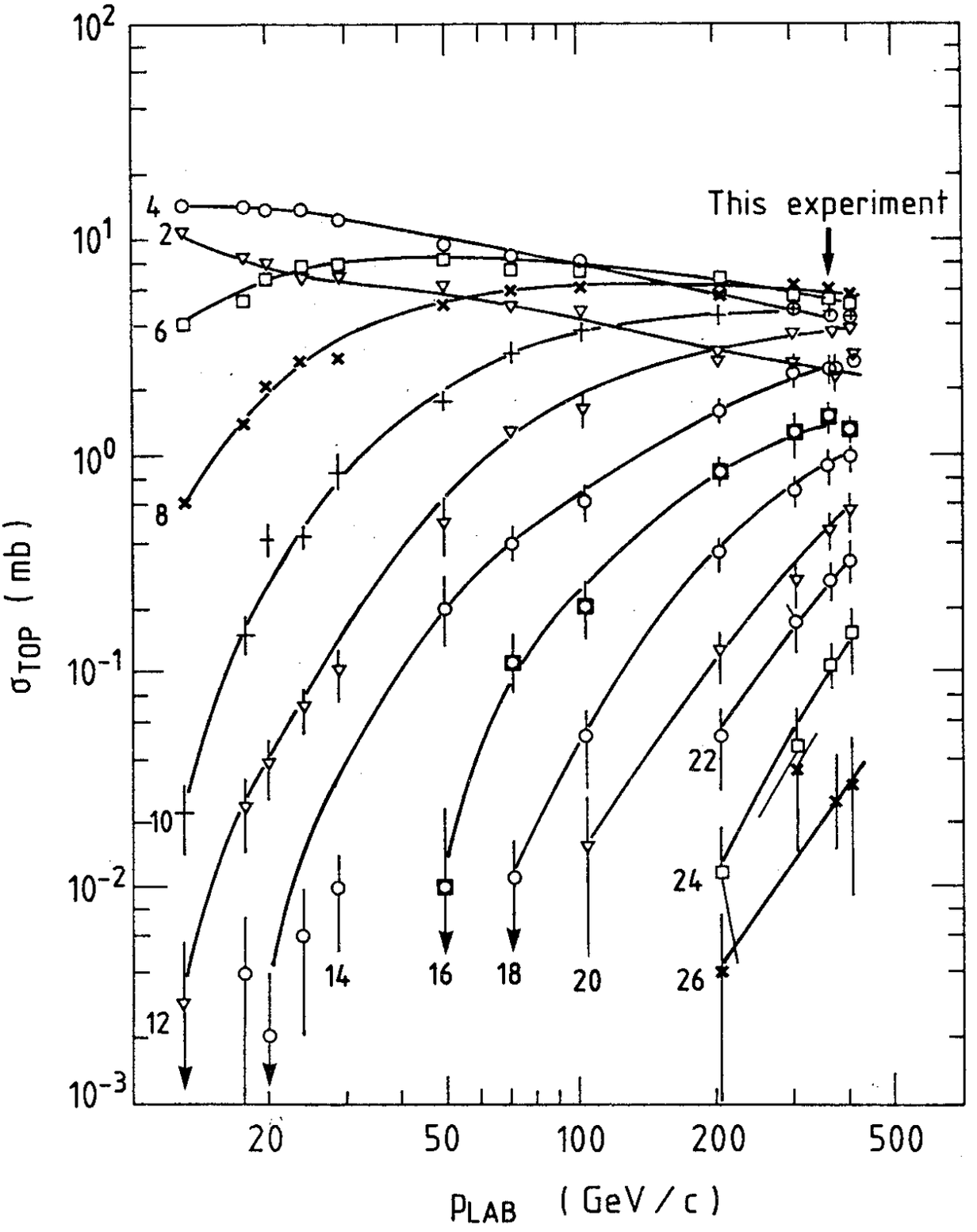
This experiment
σ_{TOP} (mb)
P_{LAB} (GeV / c)
10^2
10^1
10^0
10^{-1}
10^{-2}
10^{-3}
20
50
100
200
500
4
2
6
8
10
12
14
16
18
20
22
24
26

Fig. 5

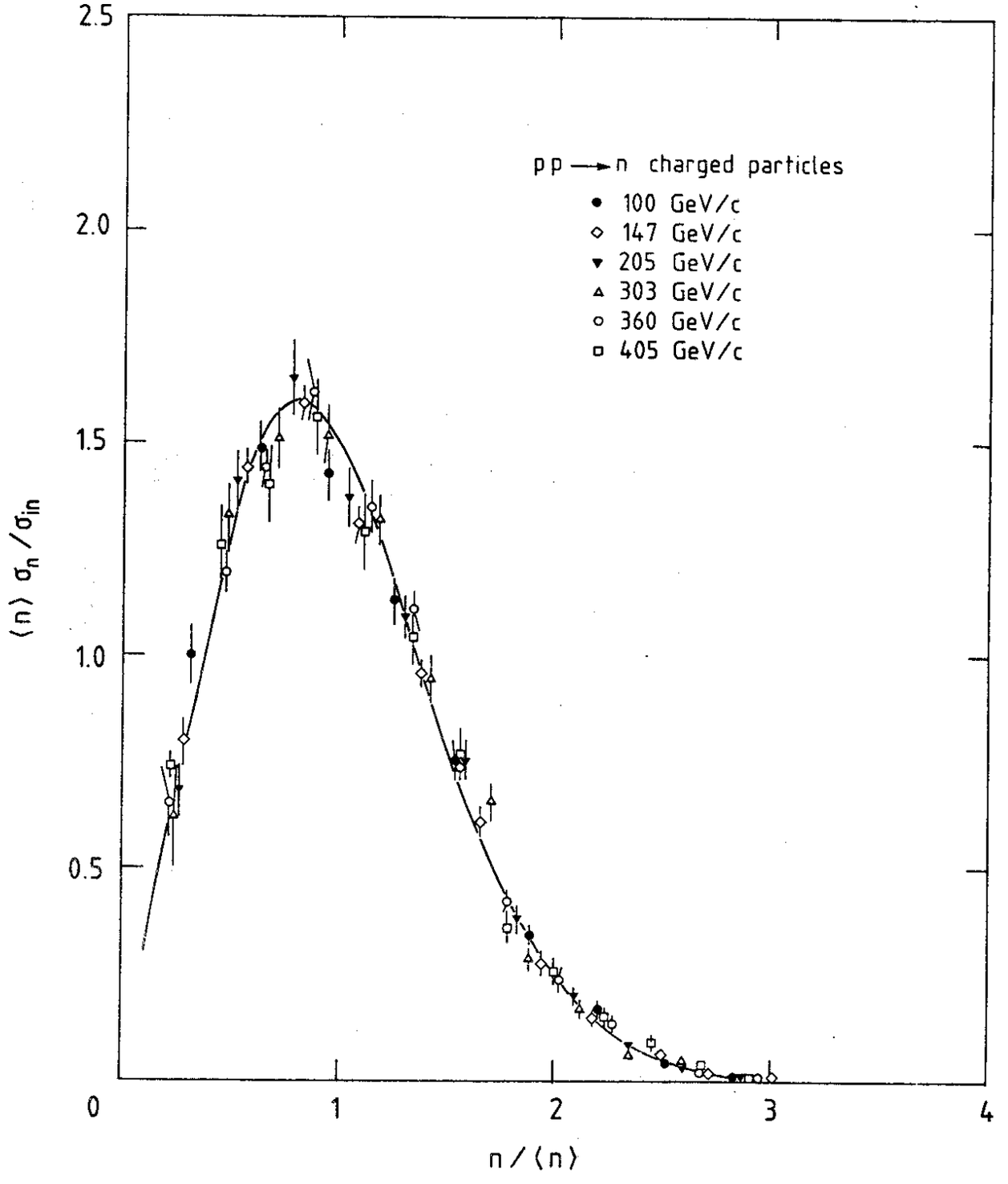
pp → n charged particles
100 GeV/c
147 GeV/c
205 GeV/c
303 GeV/c
360 GeV/c
405 GeV/c
⟨n⟩ σn / σin
n / ⟨n⟩
0
0.5
1.0
1.5
2.0
2.5
1
2
3
4

Fig. 6

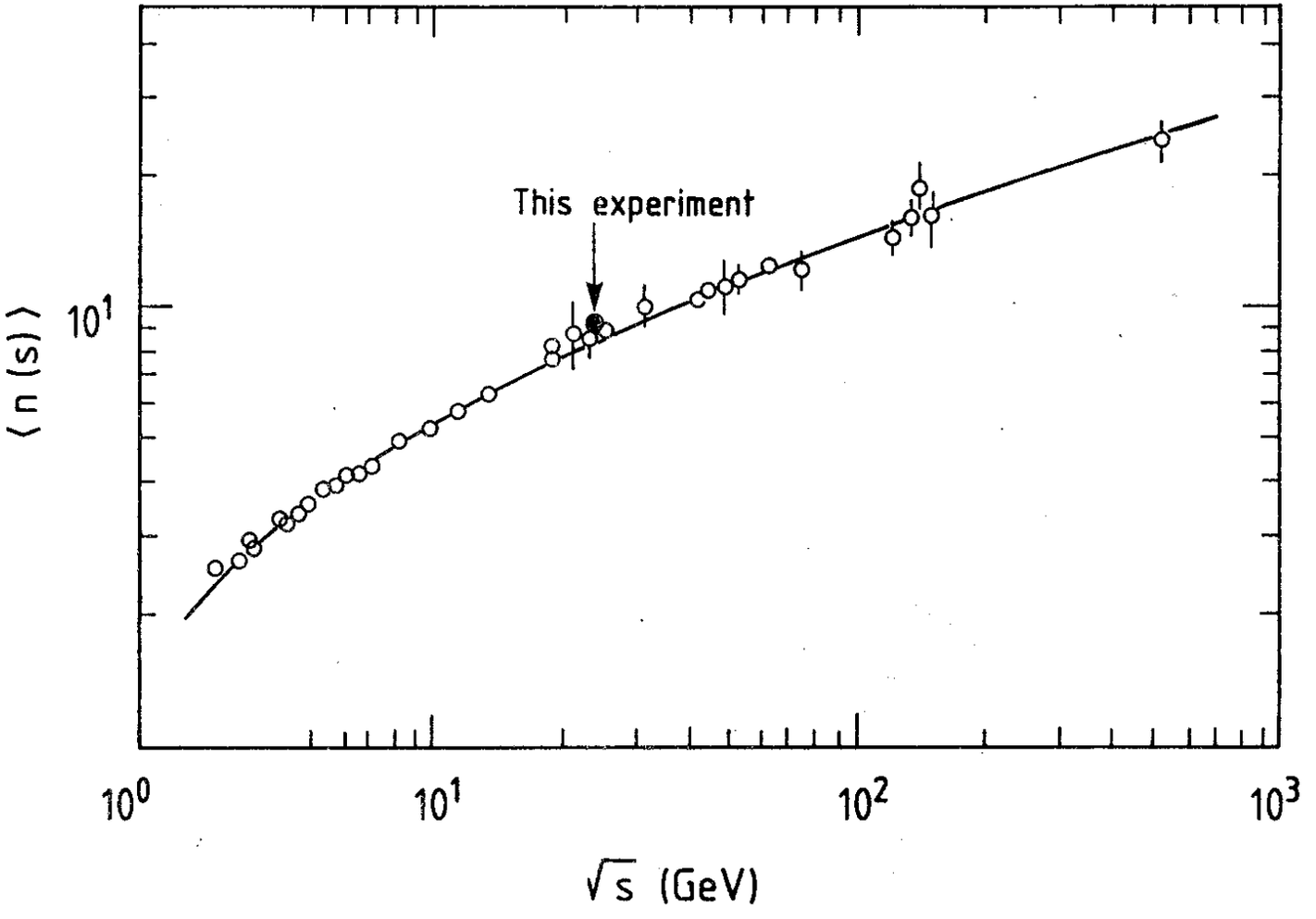

Fig. 7

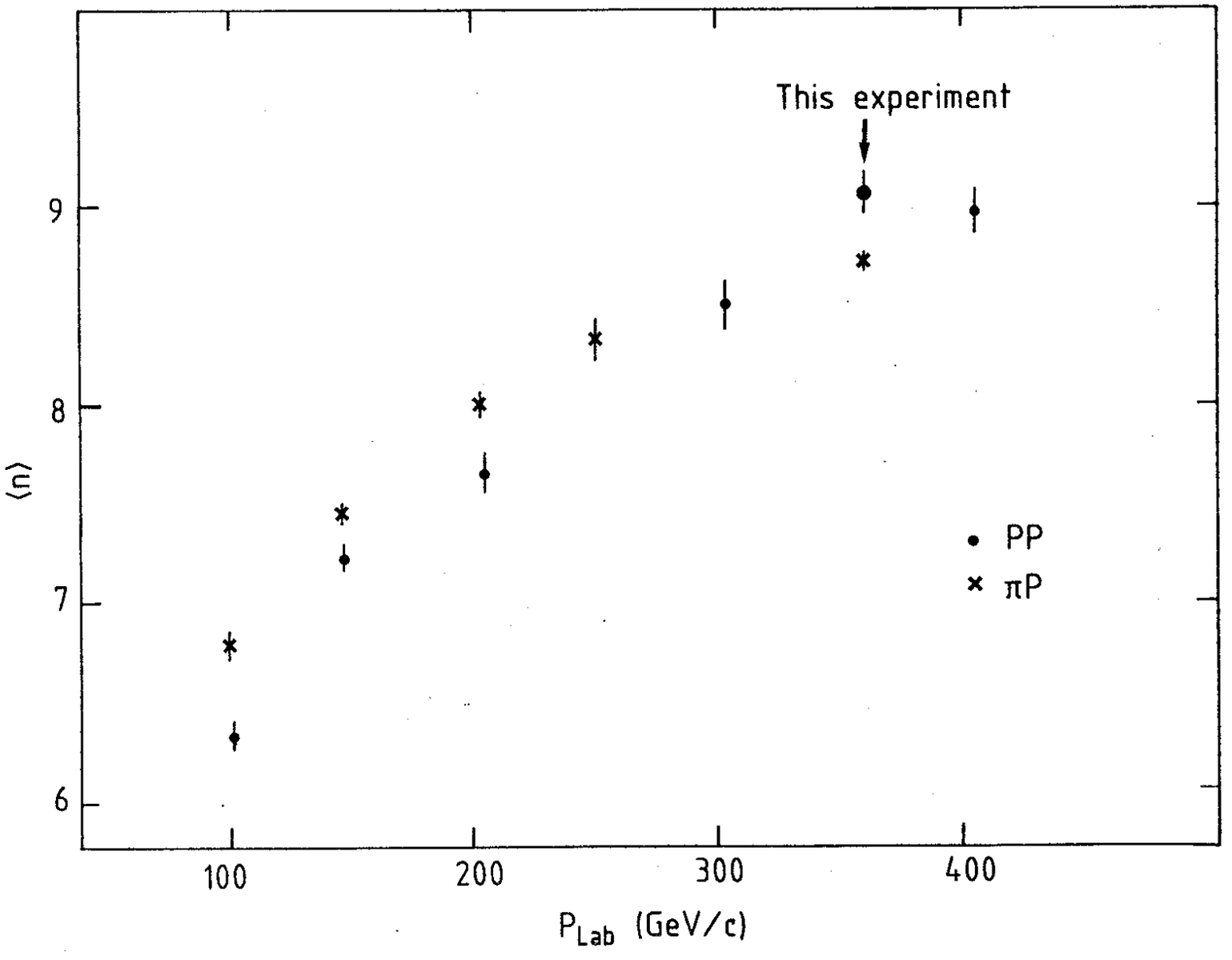

Fig. 8

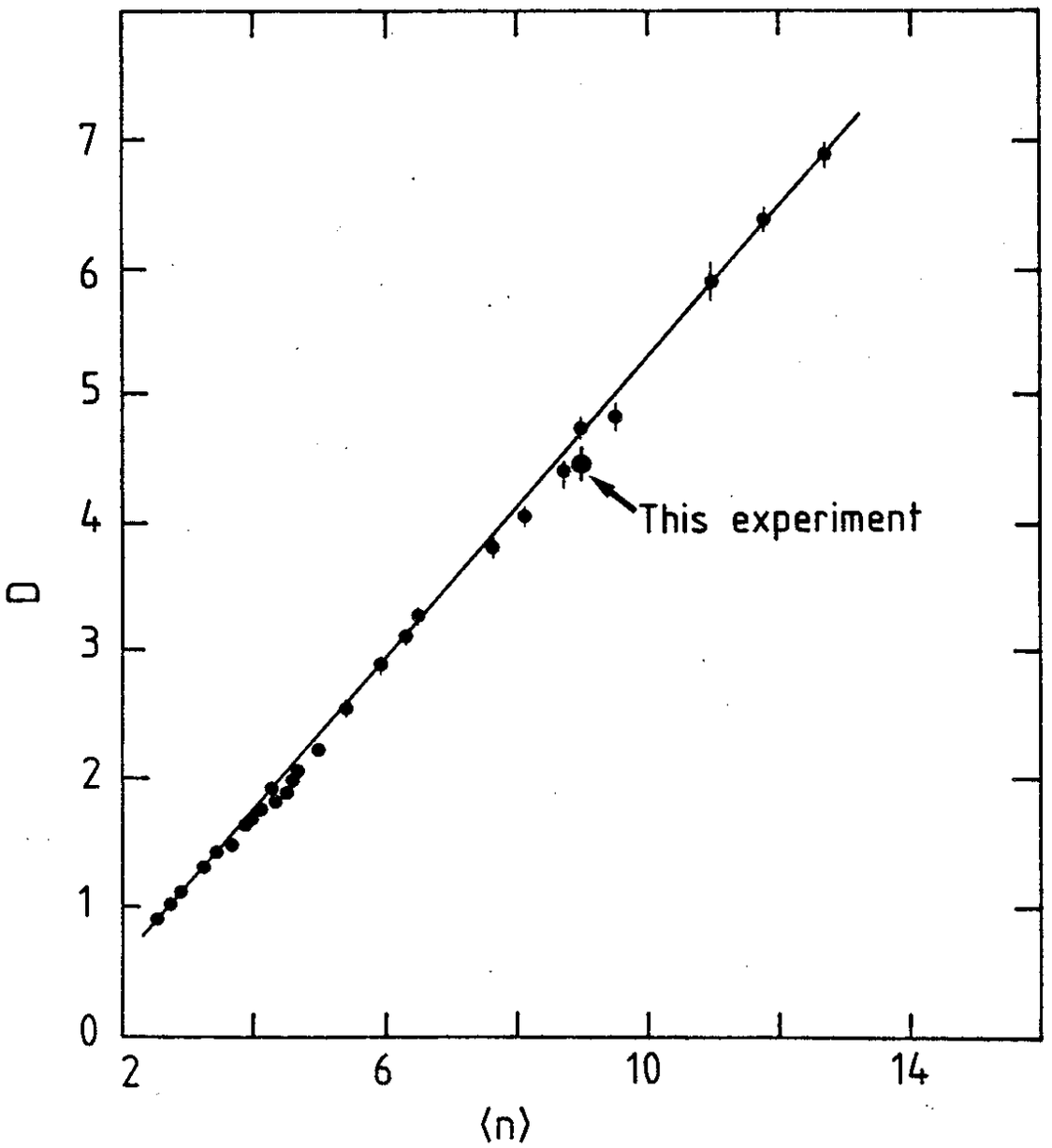

Fig.9

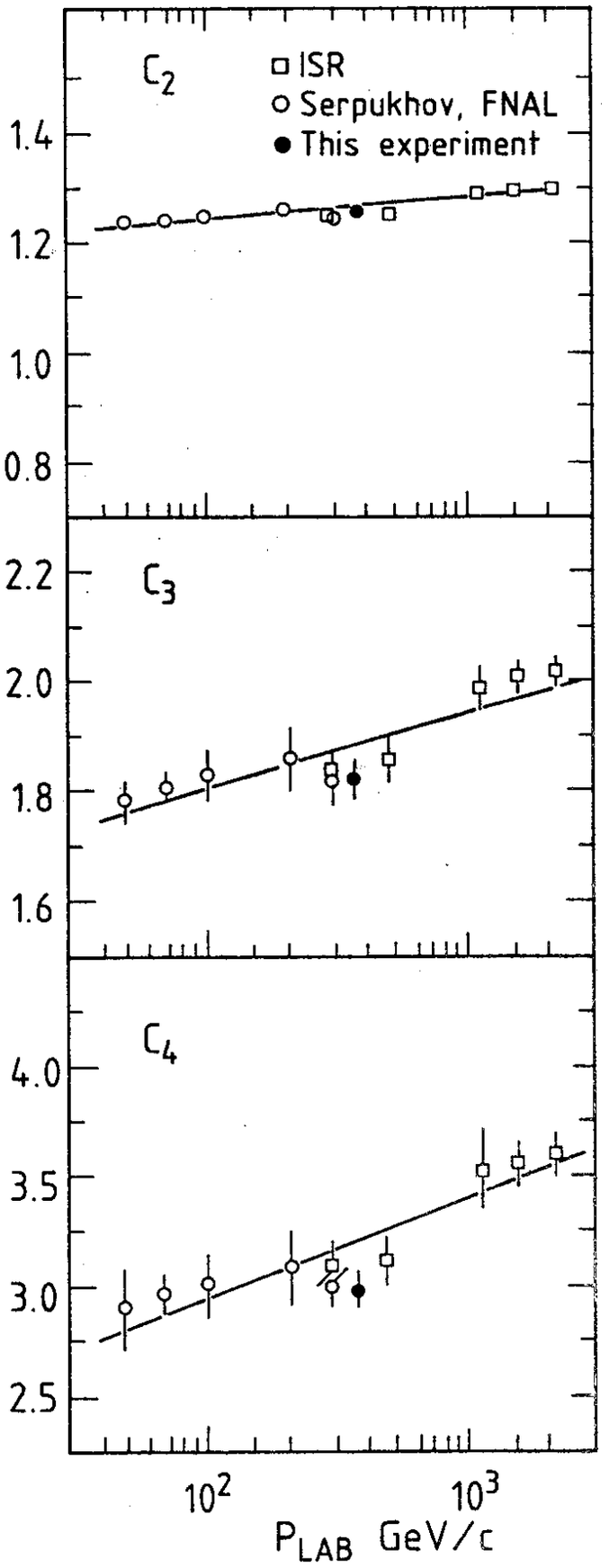
C_2
□ ISR
○ Serpukhov, FNAL
● This experiment
1.4
1.2
1.0
0.8
C_3
2.2
2.0
1.8
1.6
C_4
4.0
3.5
3.0
2.5
10^2
10^3
P_{LAB} GeV/c

Fig. 10

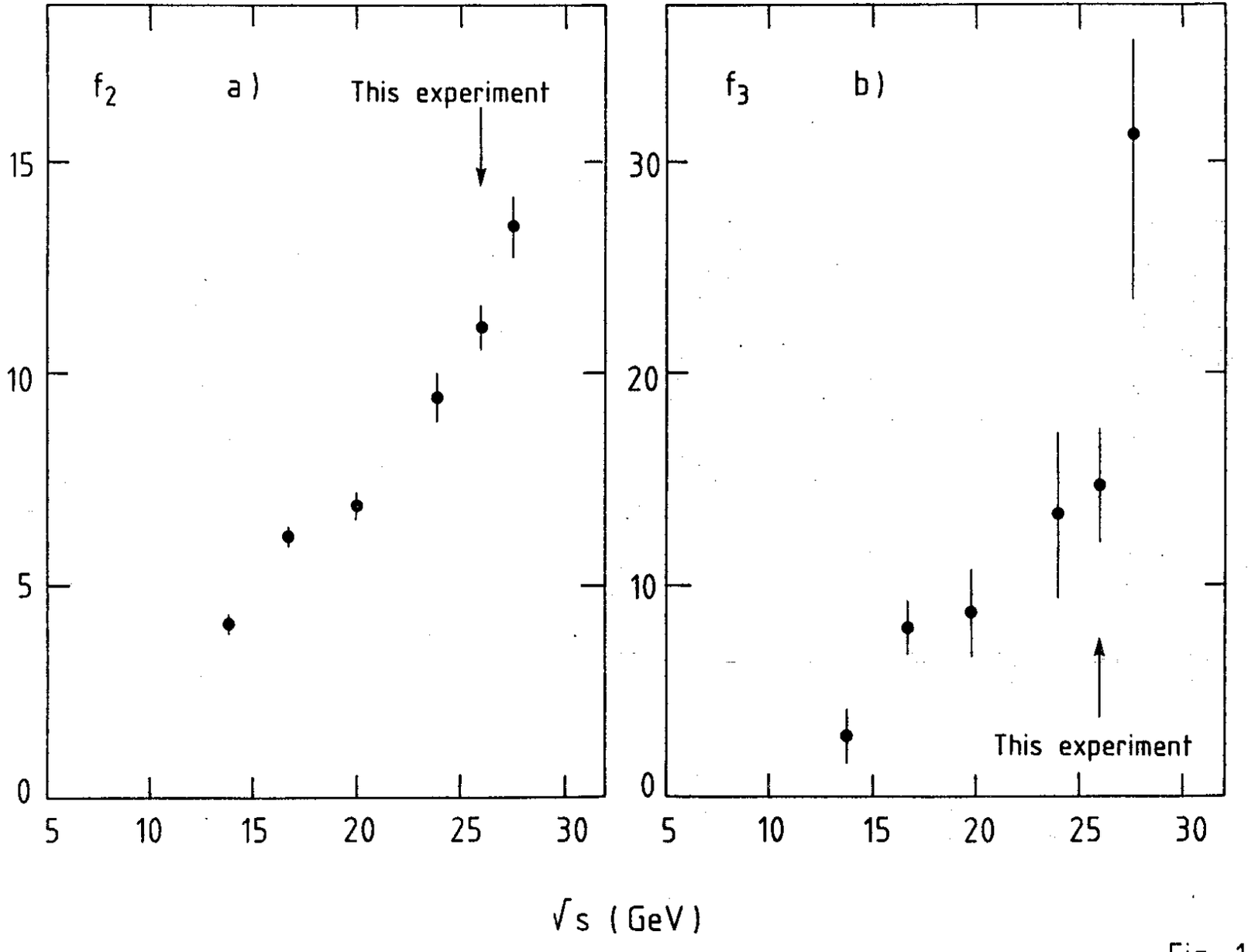
f_2
a)
This experiment
15
10
5
0
5
10
15
20
25
30
f_3
b)
30
20
10
0
This experiment
$\sqrt{s}$ (GeV)

Fig. 11